

# A LOCATION-MIXTURE AUTOREGRESSIVE MODEL FOR ONLINE FORECASTING OF LUNG TUMOR MOTION

BY DANIEL CERVONE<sup>\*</sup>, NATESH S. PILLAI<sup>\*</sup>, DEBDEEP PATI<sup>†</sup>, ROSS  
BERBECO<sup>‡</sup> AND JOHN HENRY LEWIS<sup>‡</sup>

*Harvard University<sup>\*</sup>, Florida State University<sup>†</sup>, Brigham and Women's  
Hospital, Dana-Farber Cancer Institute and Harvard Medical School<sup>‡</sup>*

Lung tumor tracking for radiotherapy requires real-time, multiple-step ahead forecasting of a quasi-periodic time series recording instantaneous tumor locations. We introduce a location-mixture autoregressive (LMAR) process that admits multimodal conditional distributions, fast approximate inference using the EM algorithm, and accurate multiple-step ahead predictive distributions. LMAR outperforms several commonly used methods in terms of out-of-sample prediction accuracy using clinical data from lung tumor patients. With its superior predictive performance and real-time computation, the LMAR model could be effectively implemented for use in current tumor tracking systems.

**1. Introduction.** Real-time tumor tracking is a promising recent development in External Beam Radiotherapy (XRT) for the treatment of lung tumors. In XRT, a compact linear accelerator is used to deliver photon radiation to the tumor locations in a narrow beam, minimizing exposure to nearby healthy tissue. As the location of the lung tumor is in constant motion due to respiration, some patients who undergo this treatment are implanted with a small metal marker (known as a fiducial) at the location of a tumor. During XRT, X-ray imaging reveals the location of the fiducial, thus providing the desired target of the radiation beam. Tumor tracking is an advanced technology that minimizes normal tissue exposure by moving the radiation beam to follow the tumor position [28, 5, 31]. However, there is a system latency of 0.1–1.0 seconds (depending on the equipment used) that causes the aperture of the radiation beam to lag behind the real-time location of the tumor. This latency is estimated empirically by comparing the motion history of the fiducial and radiation beam aperture. For tumor tracking XRT to be successful, hardware and software system latencies must be overcome by the introduction of a predictive algorithm.

---

*Keywords and phrases:* lung tumor tracking, external beam radiotherapy, nonlinear time series, mixture autoregressive process, time series motifs, likelihood approximation, multiple-step prediction

As accurate radiotherapy is essential for both minimizing radiation exposure to healthy tissue and ensuring the tumor itself is sufficiently irradiated, the subject of predicting tumor motion to overcome the system latency has received a good deal of attention in the medical community. Any possible forecasting approach must provide  $k$ -step ahead predictive distributions in real-time, where  $k$  is approximately equal to the system latency times the sampling frequency of the tumor tracking imagery. Real-time forecasting requires that a ( $k$ -step ahead) prediction be made before any further data on the tumor's motion has been recorded.

Statistical methods for tumor prediction in the literature include penalized linear models (*e.g.*, Sharp et al. [32] and many others), the Kalman filter (Murphy, Isaakson and Jalden [26]), state-space models (Kalet et al. [17]), and wavelets (Ernst, Schlaefter and Schweikard [9]); machine learning methods include kernel density estimation (Ruan and Keall [29]), support vector regression (Riaz et al. [27] and Ernst and Schweikard [10]), and neural networks (Murphy, Isaakson and Jalden [26] and Murphy and Dieterich [25]). All of these examples include simulations of out-of-sample prediction using real patient data in order to assess forecasting accuracy. Because predictive performance varies considerably from patient to patient and across different equipment configurations, of particular importance to the literature are comparisons of different prediction methods for the same set of patients with the same conditions for data preprocessing [32, 18, 11].

We propose a novel time series model which we call a location-mixture autoregressive process (LMAR). A future observation ( $Y_n$ ) given the observed history of the time series is assumed to follow a Gaussian mixture,

$$(1.1) \quad Y_n | Y_{n-1}, Y_{n-2}, \dots \sim \sum_{j=1}^{d_n} \alpha_{n,j} \mathcal{N}(\mu_{n,j}, \sigma^2),$$

where  $\sum_{j=1}^n \alpha_{n,j} = 1$ , and  $\mu_{n,j}$  is of the form

$$(1.2) \quad \mu_{n,j} = \tilde{\mu}_{n,j} + \sum_{l=1}^p \beta_l Y_{n-l}.$$

We refer to this as a location-mixture autoregressive model because the autoregressive part of the component means,  $\sum_{l=1}^p \beta_l Y_{n-l}$ , is the same for all  $j$ , and only the location parameter,  $\tilde{\mu}_{n,j}$ , changes across the components in (1.1). Our model differs from other time series models that yield mixture-normal conditional distributions (*e.g.*, the class of threshold autoregressive models (Tong and Lim [36]), including Markov-switching autoregressive models (Hamilton [13]) and the mixture autoregressive models

of Wong and Li [40]) in that  $\tilde{\mu}_{n,j}$  in (1.2) depends on an unknown subseries of the time series, at least  $p$  observations in the past. The mixture weights,  $\{\alpha_{n,j}\}$ , also depend on the entire history of the observed time series, and the number of mixture components in our model,  $d_n$ , increases with  $n$ .

Another noteworthy characteristic of our model is that all parameters in (1.1) are obtained from a single, unknown,  $(p+1) \times (p+1)$  positive definite matrix. This parsimonious parameterization is motivated in part by the need for real-time parameter estimation and forecasting. Compared with other mixture autoregressive models, LMAR is simpler to fit and admits accurate closed-form expressions for  $k$ -step ahead predictive distributions. While the data application we consider shows the promise and appeal of the LMAR model, we believe a thorough treatment of its theoretical properties (a future endeavor) is necessary before the LMAR model is a viable “off-the-shelf” method for diverse data sets.

Our model also has a useful interpretation in instantiating motifs in the time series. Motifs catalog recurring patterns in time series and are commonly used in classification and clustering of time series (Lin et al. [22]), as well as other problems for which a symbolic representation of a time series is useful (*e.g.*, association rules (Das et al. [6])). Time series motifs can also be used for forecasting, though the literature is sparse on this subject. The LMAR model is unique in that motifs are instantiated within a well-defined data-generating process, as opposed to being algorithmically extracted from the data.

Section 2 of this paper discusses the important features of the data we use. Section 3 formally introduces the LMAR model and describes parameter estimation and forecasting using principled methods that are feasible in real-time. Section 4 describes the procedure for comparing out-of-sample prediction error under our model with prediction using penalized linear models and neural networks, including the selection of model-specific hyperparameters. The results of this comparison are discussed in section 5.4, and section 6 summarizes the article and points out future directions.

**2. Tumor tracking data.** We have data on 11 patients treated at the Radiation Oncology Clinic at the Nippon Telegraph and Telephone Corporation Hospital in Sapporo, Japan. A detailed discussion of the conditions and instruments involved in the data acquisition is available in Berbeco et al. [1]. The data is derived from observations of the position of gold fiducial markers implanted into the tumors of lung cancer patients. The marker position is determined via stereoscopic x-ray imaging conducted at 30 Hz. In each of the two stereoscopic images, the marker position is automatically

detected using thresholding and edge detection. The position of the marker in these two images is used to triangulate its position in 3D space relative to the radiation beam. Data consists of tumor positions measured over one or multiple days of radiotherapy treatment delivery (range 1-12), and for multiple sequences on each day, denoted *beams*. In our data set, there are a total of 171 such distinct sequences, with lengths varying from 637 observations (about 21 seconds at 30 observations per second) to 8935 observations (about 5 minutes). Table 1 provides summary statistics for each patient’s data.

Note that this paper focuses on within-beam forecasting—that is, each beam is treated independently and there is no information sharing between patients or within different beams from the same patient. Developing methodology for combining prediction models from distinct time series (both within and across patients) is an important area for further research.

Patient	Total beams	Total time (s)	Amplitude		Period(s)	
			mean	SD	mean	SD
1	4	212.27	14.57	6.98	3.66	1.16
2	2	136.87	13.74	1.84	3.89	1.06
3	2	80.93	9.84	3.16	3.97	0.56
4	38	2502.67	8.86	1.35	2.88	0.31
5	26	2769.33	7.90	1.66	3.61	0.68
6	28	2471.93	10.07	2.51	2.58	0.55
7	11	1661.37	9.66	2.41	5.05	1.09
8	8	832.80	14.38	4.02	3.15	1.18
9	15	2599.90	11.45	1.61	3.09	0.41
10	15	3497.67	14.88	3.65	3.77	0.64
11	22	3674.77	21.81	5.05	3.38	0.52

TABLE 1

*Summary statistics for the first principal component of respiratory trace data, at the patient level*

2.1. *Features of the data.* Each observation in each sequence is a point in  $\mathbb{R}^3$ , representing the real-time 3D location of the lung tumor. The  $X$  axis is the lateral-medial (left-right) direction,  $Y$  axis is superior-inferior, and the  $Z$  axis is anterior-posterior, with all measurements in millimeters<sup>1</sup>. Figure 1 shows the motion in each dimension during the first 100 seconds of

<sup>1</sup>The origin is set to the isocenter, which is the center of rotation for the linear accelerator axis motions. During treatment, the patient is positioned so that this coincides with the centroid of the region being treated. However, there is uncertainty in determining this point, so the data is best thought of as relative tumor motion on each day.

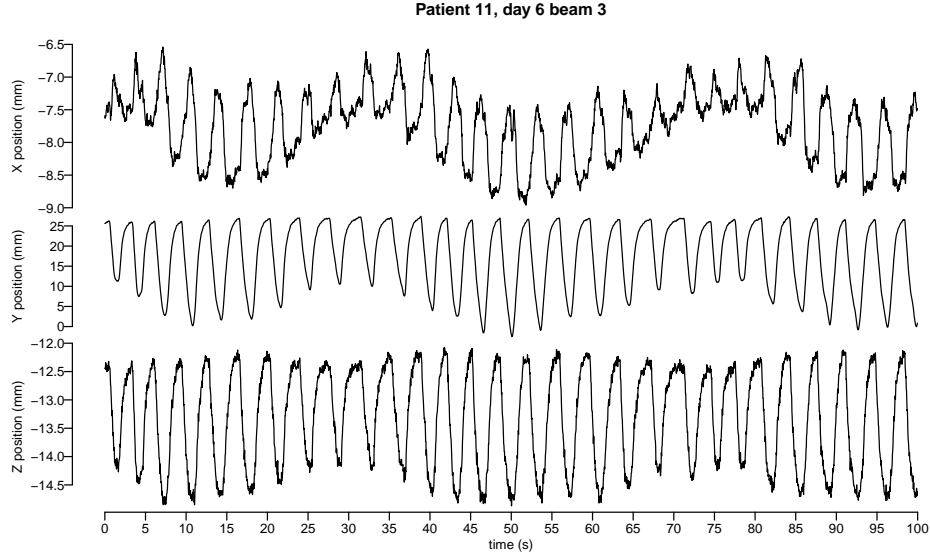
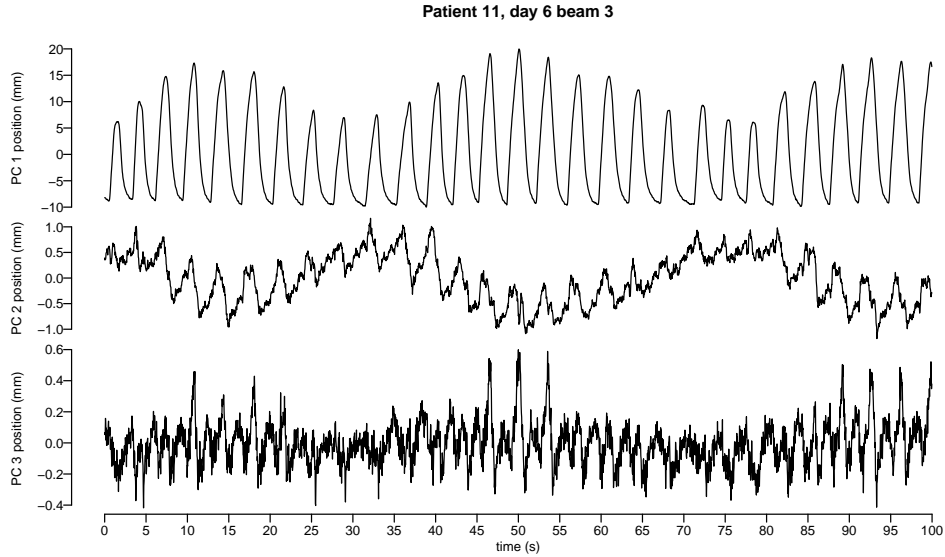


FIG 1. *Example time series of 3D locations of lung tumor. The X axis is the lateral-medial (left-right) direction, Y axis superior-inferior, and the Z axis anterior-posterior*

a particular observation sequence. As expected with respiratory motion, the pattern is approximately periodic, with inhalation closely corresponding to decreasing values in the  $Y$  direction. However, the amplitude of each breath varies considerably (in figure 1 the variation seems periodic, though this is not a typical feature of the data). The curves undergo gradual baseline location shifts, and, while it may not be visually discerned from figure 1, it is common for respiratory cycles to change periodicity, either sporadically or gradually over time. Table 1 shows the variability in period and amplitude of the respiratory traces, both within and between patients.

Due to the extremely high correlations between series of observations from different dimensions, it is useful to consider a lower-dimensional representation of the 3D process. Transforming each 3D sequence into orthogonal components using principal component analysis (PCA) loads the periodic respiratory dynamics onto the first component, representing about 99% of the total variance in the 3D data. The last two principal components still exhibit some periodic behavior, but the signal is weak relative to the noise (see figure 2). In addition to dimension reduction and useful interpretability, the PCA transformation prevents any loss of statistical efficiency if models are fit independently for each component. Ruan and Keall [29] compared

FIG 2. *Time series of principal components*

independent-component prediction before and after PCA using kernel density estimation, finding smaller 3D root mean squared prediction error when using the PCA-transformed data for prediction. When comparing several algorithms for predicting lung tumor motion, both Ernst et al. [11] and Krauss, Nill and Oelfke [18] use the principal components, then transform their predictions to the original linear basis of the data.

For the remainder of this study, we focus on modeling the first principal component only, as it encodes such a large portion of the system dynamics. Extension to a model involving all the three components is straightforward.

**2.2. Time series motifs.** Another distinctive feature of this data is that, for each patient, individual breaths tend to cluster into a few distinct shapes that characterize the trajectory of the breath, including to some extent its length and amplitude. Figure 3 shows three distinct patterns that breathing cycles in this particular segment of the observation sequence follow. The blue curves have a dramatically different shape, owing to a pause at the end of the exhale before inhaling the next breath. The red curves reach their maximum later in the relative length of their cycle than the orange curves, thus corresponding to a more gradual inhale.

Because the data is quasi-periodic, it is useful to look at short patterns

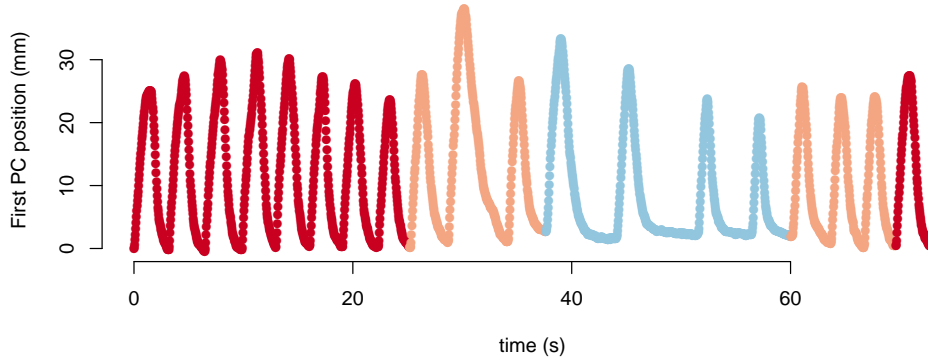


FIG 3. For the first principal component of patient 11, day 7, beam 2, breaths are clustered by the similarity of their trajectory. It is not readily apparent in this figure, but for the red curves the peak of the curve happens 10% later in its cycle than for the orange curves.

that recur at possibly irregular intervals, which we call motifs. Figure 4 highlights different motion patterns in the first principal component at the end of the exhale (start of the inhale) for a particular observation sequence. The motif instances highlighted appear to be heartbeats, which affect the location of the tumor differently depending on the real-time location of the tumor relative to the heart. Areas boxed by lines of the same color resemble one another.

Formally, a *time series* is an ordered sequence of real numbers  $\{Y_i \in \mathbb{R}, i = 0, \pm 1, \pm 2, \dots\}$  measured at regular, equally spaced intervals. Also, a *subseries* of length  $p + 1$  is a subset of a time series  $\{Y_i, i = 0, \pm 1, \dots\}$  comprised of consecutive observations,  $Y_i, Y_{i+1}, \dots, Y_{i+p}$ . For notational ease, we will denote subseries as  $Y_{i:(i+p)}$ , or equivalently  $Y_{i+0:p}$ . Lastly, a subseries  $Y_{i+0:p}$  is a *motif* if for some  $j \neq i$ , we have  $Y_{i+0:p} \rightarrow Y_{j+0:p}$ , where  $\rightarrow$  is some relation that corresponds to closeness or similarity. Here,  $Y_{j+0:p}$  is called an *instance* of the motif  $Y_{i+0:p}$ .

Lin et al. [22] first introduced motifs for real-valued time series for dimension reduction, and for providing features useful for time series clustering and classification. Much of the literature on motif recovery focuses on algorithms for extracting and/or clustering motifs (*e.g.* Chiu, Keogh and Lonardi [4] and Mueen et al. [24]), as well as event detection and time series classification (Ye and Keogh [41], Tanaka, Iwamoto and Uehara [33], and Fu [12] and references therein). Less work has been done specifically on applications of time series motifs to forecasting. Schlüter and Conrad [30] consider motif representations of multiple inter-correlated time series, and assuming a Markov structure on motif sequences in each series, predict future values

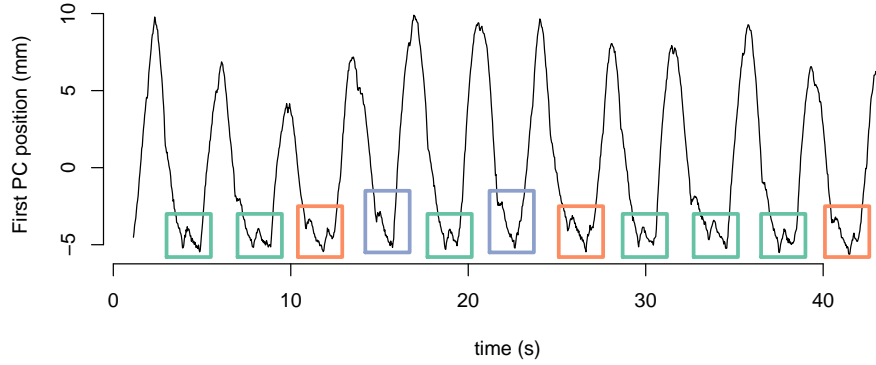


FIG 4. *Short motifs (color-coded) on the first principal component of patient 10, day 1, beam 3. The pattern of motion highlighted in these motifs is most likely caused by the patient's heartbeat.*

within a particular series using values from a correlated exogenous time series. Truong and Anh [38] present a forecasting algorithm that combines a time series' most prevalent motif and neural networks.

Our approach, given in section 3, is novel in that motifs are actually represented in a well-defined data-generating process. The relations that instantiate motifs ( $\rightarrow$ ), as well as the conditional distributions of the time series data, share a common parameterization that can be inferred from the data.

**2.3. Forecasting with time series motifs: a graphical example.** Observing repeated motifs within each time series in the data suggests a modeling/prediction framework that leverages this structure. In general, if the time series is currently within an instance of a motif that we have observed previously in the data, then the shape of this motif should inform our predictions of future observations in concert with the time series' most recent behavior.

To informally illustrate this basic idea, consider predicting 0.4s (12 steps) ahead for the first principal component of the curve displayed in figure 2. We have observed 100 seconds of the process, and it appears as though we have just observed the start of the exhale (the current observation at time  $t = 100$  seconds, as well as the previous 12 observations, are colored orange in figure 5). If we instantiate a motif corresponding to our current position



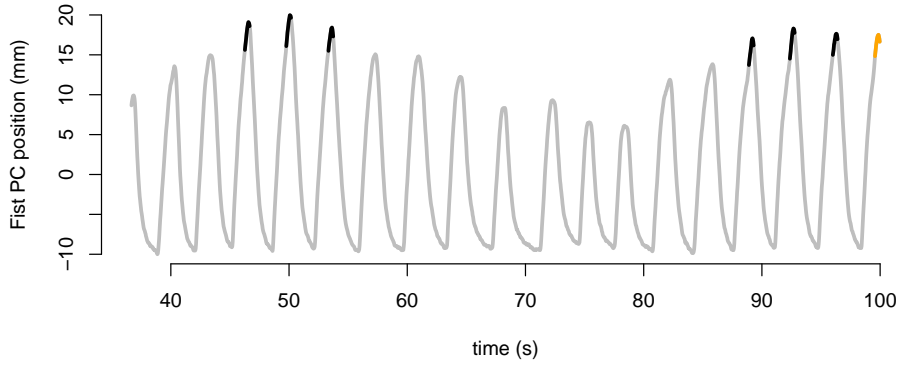


FIG 5. *The current observation, as well as the most recent 12 observations, are in orange. Previous instances of a corresponding motif are highlighted in black.*

and recent history, the more distant past reveals previous appearances of this motif (colored in black for the previous 60 seconds of the time series in figure 5). In this example, subseries of this time series of length 13 were identified as instances of this motif if the tenth point has the largest magnitude (above 15 mm), and the 11<sup>th</sup>–13<sup>th</sup> points are decreasing.

Then, to predict an observation 0.4s ahead of the current observation window, we take a weighted average of the points observed 0.4s after the end of the previous instances of this motif. Figure 6 shows the trajectories (in gray) of the time series after the end of the motif instances highlighted in black in figure 5. The current trajectory of the process is shown in orange, with a point giving the actual value 0.4s in the future. The gray curves provide reasonable forecasts for the future evolution of the time series, and indeed the actual future value is close to where these trajectories predict.

### 3. Location-mixture autoregressive processes.

3.1. *A model for the data-generating process.* In this section, we present the location-mixture autoregressive process with parameters  $(p, \Sigma)$  (abbreviated LMAR( $p, \Sigma$ )). Let  $\{Y_i, i = -m, \dots, n\}$  be a time series. Also, assume  $\Sigma$  is a  $(p + 1) \times (p + 1)$  symmetric, nonnegative definite matrix, where  $\Sigma_{11}$  is the upper-left  $p \times p$  submatrix,  $\Sigma_{22}$  is the single bottom-right element, and  $\Sigma_{21}$  and  $\Sigma_{12}$  are the respective off-diagonal row and column vectors.  $p$  is assumed to be fixed and known. For notational ease, let  $\gamma = \Sigma_{11}^{-1}\Sigma_{12}$ ,

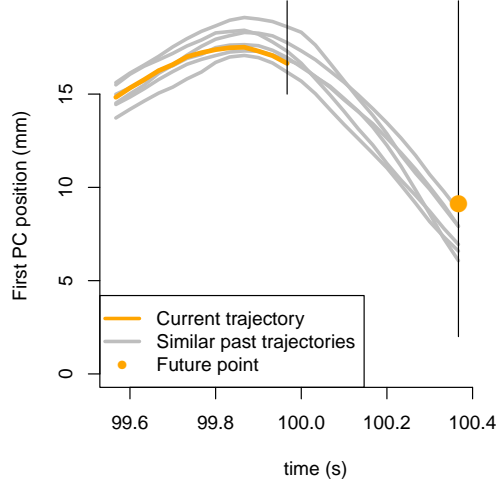


FIG 6. *The recent history of the process (orange line) instantiates a motif. Previous instances of this motif, and their subsequent evolutions, are in gray and provide reasonable predictions for future points (orange dot).*

$\sigma^2 = \Sigma_{22} - \gamma' \Sigma_{12}$ , and  $\mathcal{J}_n = \{p+1, \dots, n+m-p\}$ . Lastly, let

$$V_{ij} = \begin{pmatrix} Y_{i-p} - Y_{i-j-p} \\ \vdots \\ Y_{i-2} - Y_{i-j-2} \\ Y_{i-1} - Y_{i-j-1} \end{pmatrix}.$$

As in (1.1), we assume the distribution of  $Y_i$  given  $Y_{-m}, \dots, Y_{i-1}$  is a normal mixture,

$$Y_i | Y_{(-m):(i-1)} \sim \sum_{j \in \mathcal{J}_i} \alpha_{i,j} N(\mu_{i,j}, \sigma^2),$$

where

$$\alpha_{i,j} = \frac{\exp\left(-\frac{1}{2} V_{ij}' \Sigma_{11}^{-1} V_{ij}\right)}{\sum_{l \in \mathcal{J}_i} \exp\left(-\frac{1}{2} V_{il}' \Sigma_{11}^{-1} V_{il}\right)} \text{ and } \mu_{i,j} = Y_{i-j} + \gamma' V_{ij}.$$

It may also be illustrative to write the distribution function of  $Y_i|Y_{(-m):(i-1)}$ :

$$(3.1) \quad F(y|Y_{(-m):(i-1)}) = \sum_{j \in \mathcal{J}_i} \Phi \left( \frac{y - (Y_{i-j} + \gamma' V_{ij})}{\sigma} \right) \left( \frac{\exp \left( -\frac{1}{2} V_{ij}' \Sigma_{11}^{-1} V_{ij} \right)}{\sum_{l \in \mathcal{J}_i} \exp \left( -\frac{1}{2} V_{il}' \Sigma_{11}^{-1} V_{il} \right)} \right),$$

where  $\Phi$  denotes the standard normal CDF. Thus our normal mixture distribution for  $Y_i|Y_{(-m):(i-1)}$  has  $|\mathcal{J}_i|$  different mean components, equal variance across components ( $\sigma^2$ ), and data-driven mixture weights. Note that the indexing set  $\mathcal{J}_i$  ensures any component of  $Y_{(-m):(i-1)}$  appears in  $Y_{i-j} + \gamma' V_{ij}$  at most once. We assume (3.1) for all  $i \geq 0$ , but we do not make any distributional assumptions about  $Y_{(-m):(-1)}$ .

As  $\Sigma$  parameterizes the entire mixture distribution, the component means and mixture weights are linked through a common parameter which encourages self-similarity in the data-generating process. If two subseries,  $Y_{(i-p):(i-1)}$  and  $Y_{(i-j-p):(i-j-1)}$  resemble one another in that  $V_{ij}' \Sigma_{11}^{-1} V_{ij}$  is small, then we have a large weight on the mixture component with mean  $Y_{i-j} + \gamma' V_{ij}$ . This means that the next observation of the process,  $Y_i$ , is centered near a previous value of the series  $Y_{i-j}$  inasmuch as the subseries of observations preceding  $Y_i$  and  $Y_{i-j}$  have a similar shape.

The model (3.1) specifies the role of time series motifs in the data-generating process, which was informally discussed in sections 2.1 and 2.2. To illustrate this, we introduce a latent variable  $M_i$  that takes values in  $\mathcal{J}_i$ , such that for all  $j \in \mathcal{J}_i$ ,

$$(3.2) \quad \mathbb{P}(M_i = j|Y_{(-m):(i-1)}) \propto \exp(-V_{ij}' \Sigma_{11}^{-1} V_{ij}/2).$$

Then, given  $M_i = j$ , we induce the same distribution for  $Y_i$  as in (3.1) by assuming

$$(3.3) \quad Y_i|M_i = j, Y_{(-m):(i-1)} \sim N(Y_{i-j} + \gamma' V_{ij}, \sigma^2).$$

Expressions (3.2)–(3.3) define a relation that instantiates motifs, as we write  $Y_{(i-j-p):(i-j)} \rightarrow Y_{(i-p):i}$  if  $M_i = j$ . Thus, the physical interpretation of this definition of a motif is that if  $Y_{(i-p):i}$  is an instance of motif  $Y_{(i-j-p):(i-j)}$ , then  $Y_i$  should be close to  $Y_{i-j}$  if  $V_{ij}$  is near 0, with distance measured by a Gaussian kernel. It is important to note that unlike many other applications of time series motifs in the literature, here we assume that every observation is part of a motif instance in that  $M_i \in \mathcal{J}_i$  for all  $i$ . This assumption is justified by the strength of the periodicity, or self-similarity, of the data.

3.2. *Comparison with other mixture autoregressive processes.* We may compare the LMAR( $p, \Sigma$ ) to a general form of regime-switching autoregressive models, for which we can write the distribution function of  $Y_i$  conditional on all available history of the process  $Y_{(-m):(i-1)}$  as

$$(3.4) \quad F(y|Y_{(-m):(i-1)}) = \sum_{j=1}^d \alpha_{i,j} \Phi \left( \frac{y - (\beta_{0,j} + \sum_{l=1}^p \beta_{l,j} Y_{i-l})}{\sigma_j} \right),$$

where  $\sum_{j=1}^d \alpha_{i,j} = 1$  for all  $i$ . Models satisfying (3.4) can be represented in the framework of threshold autoregressive models (Tong [34], Tong and Lim [36]; see Tong [35] for a book-length treatment), which specify an indicator series  $\{M_i\}$  taking values on  $\{1, \dots, d\}$ , such that

$$(3.5) \quad Y_i = \beta_{0,M_i} + \sum_{l=1}^p \beta_{l,M_i} Y_{i-l} + \sigma_{M_i} \epsilon_i,$$

where  $\{\epsilon_i\}$  are i.i.d. standard normals. Generally,  $\{M_i\}$  is not observed, although there are notable exceptions such as the self-exciting threshold AR model of Tong and Lim [36].

A canonical model of this form is the mixture autoregressive model of Le, Martin and Raftery [21] and Wong and Li [40], which assumes  $M_i$ 's are i.i.d. and independent of  $Y$ . Another special case of (3.5) is when  $\{M_i\}$  is a Markov chain, such as in the Markov-switching autoregressive models of Hamilton [13] and McCulloch and Tsay [23]. More general stochastic structure for  $\{M_i\}$  is considered by Lau and So [20], as well as in mixture-of-experts models in the machine learning literature (Carvalho and Tanner [3]). These models seem favorable over the mixture autoregressive models of Wong and Li [40] when the data is seasonal or quasi-periodic, as is the case with the time series we consider.

The LMAR( $p, \Sigma$ ) process differs from (3.4) in that the mixture means, are given by

$$\mu_{i,j} = Y_{i-j} + \gamma' V_{ij} = Y_{i-j} + \gamma' Y_{(i-p):(i-1)} - \gamma' Y_{(i-j-p):(i-j-1)},$$

instead of  $\mu_{i,j} = \beta_{0,M_i} + \sum_{l=1}^p \beta_{l,M_i} Y_{i-l}$  as in (3.4). Thus, for LMAR( $p, \Sigma$ ), the autoregressive coefficients ( $\gamma$ ) are fixed, and the normal-mixture form of the conditional distribution is induced by a location shift that is a function of a random subseries of past observations,  $Y_{i-M_i} - \gamma' Y_{(i-M_i-p):(i-M_i-1)}$ . The normal-mixture form of (3.4), however, is induced by a mixture distribution for autoregressive coefficients of the same lagged values of the time series.

The mixture weights of the  $\text{LMAR}(p, \Sigma)$  process are also strongly data-driven, depending on the entire history of the process. Unlike many forms of mixture autoregressive models, there is no prior distribution or conditional dependence structure assumed for  $\{M_i\}$ ; the distribution of  $\{M_i\}$  is supplied entirely by the data.

Another key difference is that  $\text{LMAR}(p, \Sigma)$  does not assume a fixed number of mixture components, as is clear from (3.1). But because the same autoregressive coefficient vector ( $\gamma$ ) parameterizes all mean components  $\mu_{i,j}$ , we actually have a much smaller parameter space than all the instances of (3.4) cited above, which include the parameters for the mixture components ( $d$  vectors of length  $p + 1$  for the means) as well as for the distribution of  $\{M_i\}$ . A small parameter space is advantageous in the context of our data application as it facilitates rapid updating. Also, time constraints will not allow for any goodness-of-fit or model selection procedures for choosing structural parameters such as  $d$  or  $p$  in (3.4), or structural parameters for  $\{M_n\}$ . The only structural parameter in the  $\text{LMAR}(p, \Sigma)$  model is  $p$ , and in our analysis of this data set we found that predictive distributions were quite stable for different choices of  $p$ .

The most important distinction of the  $\text{LMAR}(p, \Sigma)$  model is the existence of good approximations for  $k$ -step ahead predictive distributions, for  $k \leq p$ , which are given in section 3.4. Closed form predictive distributions for  $k > 1$  are not available for many models of the form (3.4) (the exception is the Markov-switching autoregressive models of Hamilton [13], for a discussion see Krolzig [19]). Wong and Li [40] recommend Monte Carlo estimates of  $k$ -step ahead predictive distributions, although Boshnakov [2] finds for them a closed-form representation as a normal mixture. Calculating the mixture component parameters for moderate  $k$ , however, is quite laborious. For the general model (3.4), De Gooijer and Kumar [7] discuss the difficulty in  $k$ -step ahead forecasting and question whether predictive performance is improved over classes of linear times series models (also see Tong and Moeanaddin [37] for a discussion of the robustness of medium-to-long range forecasts using threshold autoregressive models).

**3.3. Parameter Estimation.** Because it is desirable to adjust radiotherapy treatments in real-time to the patient's breathing pattern, we seek estimation procedures that are fast enough to run online (in less than a few seconds). As a general rule, this favors approximate closed-form solutions to estimating equations over exact numerical or Monte Carlo methods. To estimate  $\Sigma$ , which is the only unknown parameter of this model, we take a conditional likelihood approach based on the conditional distribution

$Y_{0:n}|Y_{(-m):(-1)}$ . We assume the full-data likelihood can be written as

$$L(\psi, \Sigma) = L_1(\psi, \Sigma)L_2(\Sigma),$$

where  $L_1(\psi, \Sigma) \propto \mathbb{P}(Y_{(-m):(-1)}; \psi, \Sigma)$  and  $L_2(\Sigma) \propto \mathbb{P}(Y_{0:n}|Y_{(-m):(-1)}; \Sigma)$ . The distribution of the first  $m$  observations, and thus  $L_1$ , is left unspecified, and all information for  $\Sigma$  comes from  $L_2$ . If  $L_1$  depends on  $\Sigma$ , there will be some loss of efficiency when using only  $L_2$  for inference versus the complete-data likelihood, though under mild conditions the maximum conditional likelihood estimate is consistent and asymptotically efficient (Kalbfleisch and Sprott [16]).

The conditional likelihood,  $L_2(\Sigma)$ , can be written:

$$(3.6) \quad L_2(\Sigma) = \prod_{i=0}^n \frac{1}{\sigma} \left[ \sum_{j \in \mathcal{J}_i} \exp \left( -\frac{1}{2\sigma^2} (Y_i - Y_{i-j} - \gamma' V_{ij})^2 \right) \times \left( \frac{\exp(-V_{ij}' \Sigma_{11}^{-1} V_{ij}/2)}{\sum_{l \in \mathcal{J}_i} \exp(-V_{il}' \Sigma_{11}^{-1} V_{il}/2)} \right) \right].$$

To maximize (3.6), we augment the data to  $\{Y_{0:n}, M_{0:n}\}$ , with  $M_i$  as in (3.2). This invites the use of the Expectation-Maximization (EM) algorithm (Dempster, Laird and Rubin [8]) to estimate  $\Sigma$ . The augmented-data (complete-data) conditional likelihood is

$$L_{2,\text{com}}(\Sigma) = \prod_{i=0}^n \frac{1}{\sigma} \prod_{j \in \mathcal{J}_i} \left[ \exp \left( -\frac{1}{2\sigma^2} (Y_i - Y_{i-j} - \gamma' V_{ij})^2 \right) \times \left( \frac{\exp(-V_{ij}' \Sigma_{11}^{-1} V_{ij}/2)}{\sum_{l \in \mathcal{J}_i} \exp(-V_{il}' \Sigma_{11}^{-1} V_{il}/2)} \right) \right]^{\mathbf{1}[M_i=j]}.$$

This can be simplified further. Let  $W'_{ij} = (V'_{ij} \quad Y_i - Y_{i-j})$ , and recalling the notation for  $\sigma$  and  $\gamma$ , we have

$$(3.7) \quad L_{2,\text{com}}(\Sigma) = \prod_{i=0}^n \frac{\exp \left( -\frac{1}{2} \sum_{j \in \mathcal{J}_i} \mathbf{1}[M_i = j] W'_{ij} \Sigma^{-1} W_{ij} \right)}{\sigma \sum_{l \in \mathcal{J}_i} \exp(-V'_{il} \Sigma_{11}^{-1} V_{il}/2)}.$$

The term  $\sum_{l \in \mathcal{J}_i} \exp(-V'_{il} \Sigma_{11}^{-1} V_{il}/2)$  can be viewed as an approximation of a Gaussian integral; if we assume that, for all  $i$ ,  $\{V_{il}, l \in \mathcal{J}_i\}$  resemble  $|\mathcal{J}_i|$

i.i.d. draws from some distribution  $V \sim N(0, \Omega)$ , then we have

$$\begin{aligned}
 \sum_{l \in \mathcal{J}_i} \exp(-V'_{il} \Sigma_{11}^{-1} V_{il}/2) &\approx |\mathcal{J}_i| \int \exp(-V' \Sigma_{11}^{-1} V/2) \frac{\exp(-V' \Omega^{-1} V/2)}{(2\pi)^{p/2} |\Omega|^{1/2}} dV \\
 &= |\mathcal{J}_i| \left( \frac{|(\Sigma_{11}^{-1} + \Omega^{-1})^{-1}|}{|\Omega|} \right)^{1/2} \\
 (3.8) \quad &= |\mathcal{J}_i| \left( \frac{|\Sigma_{11}|}{|\Sigma_{11} + \Omega|} \right)^{1/2}.
 \end{aligned}$$

Noting that  $\sigma|\Sigma_{11}|^{1/2} = |\Sigma|^{1/2}$ , and ignoring multiplicative constants, we arrive at an approximate augmented-data conditional likelihood

$$L_{2,\text{com}}(\Sigma) \approx \left( \frac{|\Sigma_{11} + \Omega|}{|\Sigma|} \right)^{(n+1)/2} \exp \left( -\frac{1}{2} \sum_{i=0}^n \sum_{j \in \mathcal{J}_i} \mathbf{1}[M_i = j] W'_{ij} \Sigma^{-1} W_{ij} \right).$$

Typically  $\Sigma_{11} \ll \Omega$ , meaning

$$\begin{aligned}
 \partial(\log(|\Sigma_{11} + \Omega|) - \log(|\Sigma|)) &= \text{Tr}((\Sigma_{11} + \Omega)^{-1} \partial \Sigma_{11}) - \text{Tr}(\Sigma^{-1} \partial \Sigma) \\
 &\approx -\text{Tr}(\Sigma^{-1} \partial \Sigma)
 \end{aligned}$$

as  $\partial \log(|\Sigma|)$  dominates  $\partial \log(|\Sigma_{11} + \Omega|)$ . This justifies the approximation  $\log(|\Sigma_{11} + \Omega|) - \log(|\Sigma|) \approx -\log(|\Sigma|)$  in the augmented-data conditional log-likelihood, as it will admit nearly the same maximizer. Thus, we have

$$(3.9) \quad \log(L_{2,\text{com}}(\Sigma)) \approx -\frac{n+1}{2} \log(|\Sigma|) - \frac{1}{2} \sum_{i=0}^n \sum_{j \in \mathcal{J}_i} \mathbf{1}[M_i = j] W'_{ij} \Sigma^{-1} W_{ij}.$$

While (3.9) is much easier to work with than the logarithm of the exact conditional likelihood (3.7), the assumptions of this approximation are somewhat tenuous. Under this model (3.1), both conditional and marginal distributions of observations at each time point follow a normal mixture, meaning for  $l$  randomly chosen in  $\mathcal{J}_i$ , we have a difference of normal mixtures (itself a normal mixture) for  $V_{il}$ , instead of i.i.d. normals as (3.8) suggests. We nevertheless proceed with approximation (3.9) in place of (3.7), noting that convergence of the EM algorithm needs to be more carefully monitored in this instance.

At each iteration of the EM algorithm, we maximize the so-called Q function

$$\begin{aligned}
 Q^{(t)}(\Sigma) &= \mathbb{E}_{\Sigma^{(t)}}[\log(L_{2,\text{com}}(\Sigma)) | Y] \\
 (3.10) \quad &\approx -\frac{n+1}{2} \log(|\Sigma|) - \frac{1}{2} \sum_{i=0}^n \sum_{j \in \mathcal{J}_i} \omega_{ij} W'_{ij} \Sigma^{-1} W_{ij},
 \end{aligned}$$

with  $\Sigma^{(t)} = \operatorname{argmax}(\mathcal{Q}^{(t-1)}(\Sigma))$  and  $\omega_{ij} = \mathbb{E}_{\Sigma^{(t)}}[\mathbf{1}[M_i = j]|Y]$ . Clearly,

$$\omega_{ij} = \frac{\exp(-W'_{ij}[\Sigma^{(t)}]^{-1}W_{ij}/2)}{\sum_{l \in \mathcal{J}_i} \exp(-W'_{lj}[\Sigma^{(t)}]^{-1}W_{lj}/2)}.$$

The maximizer of (3.10) can be found in closed form as a weighted sample covariance matrix,

$$(3.11) \quad \Sigma^{(t+1)} = \frac{1}{n+1} \sum_{i=0}^n \sum_{j \in \mathcal{J}_i} \omega_{ij} W_{ij} W'_{ij}$$

Again, due to several different approximations used in maximizing the original conditional likelihood (3.6), it is necessary to monitor the convergence to a suitable (if slightly sub-optimal) solution, as the log-likelihood is not guaranteed to increase at each iteration.

**3.4. A prediction model for fast implementation.** Exact closed-form expressions for  $k$ -step ahead predictive distributions are not available for the model (3.1). Because of the need for real-time forecasting of many steps ahead, we explore approximations to  $k$ -step ahead predictive distributions that are available in closed-form. An immediate approach to doing so is to explore whether the approximate complete-data conditional log-likelihood used for inference (3.9) corresponds to a probabilistic model (perhaps misspecified) that admits closed form predictive distributions. In other words, if the previous section derives an approximate log-likelihood (3.9) from an exact model (3.1), here we treat (3.9) as exact and explore corresponding approximate models.

Let  $Z_i = (Y_{i-p} \dots Y_{i-1} \ Y_i)'$  for  $0 \leq i \leq n$ . Since  $W_{ij} = Z_i - Z_j$ , we may arrive at the likelihood expression (3.9) by assuming  $Z_i \sim \mathcal{N}(Z_{i-M_i}, \Sigma)$  independently. This is obviously a misspecification, since for any  $k \leq p$ ,  $Z_i$  and  $Z_{i+k}$  contain duplicate entries and thus cannot be independent. But assuming the  $\{Z_i\}$  independent, and further assuming  $\mathbb{P}(M_i = j) = 1/|\mathcal{J}_i|$  independently for all  $i$ , we can write the (conditional) likelihood for a independent multivariate normal mixture model, denoted  $L_a$  to distinguish from  $L_{2,\text{com}}$ :

$$(3.12) \quad L_a(\Sigma) = \prod_{i=0}^n \prod_{j \in \mathcal{J}_i} \left[ |\Sigma|^{-1/2} \exp \left( -\frac{1}{2} W'_{ij} \Sigma^{-1} W_{ij} \right) \right]^{\mathbf{1}[M_i=j]}.$$

Indeed, we see that  $L_a(\Sigma)$  is equal to the approximation of  $L_{2,\text{com}}(\Sigma)$  given in (3.9). Thus, the misspecified independent mixture model for  $Z_i$  yields the



same likelihood ( $L_a$ ) as the approximation to  $L_2$ , the exact (conditional) likelihood corresponding to the data-generating process. Also, recall that  $M_i = j$  denotes  $Z_i$  as an instance of motif  $Z_j$ . The implied relation in (3.12) is that

$$(3.13) \quad Z_j \rightarrow Z_i \text{ if } Z_i | Z_j \sim N(Z_j, \Sigma),$$

and indeed this relation is closely connected to the one defined in (3.3) (they appear equivalent, as (3.3) is recovered by assuming  $Z_i | Z_j \sim N(Z_j, \Sigma)$ , and then working the conditional distribution  $Y_i | Y_{(-m):(i-1)}$ . However, for (3.13) to hold for all  $i$  requires the impossible assumption of  $Z_i$  being independent of  $Z_{i-1}$ , while the relation in (3.3) does not).

The corresponding  $Q$  function for this complete-data conditional likelihood (3.12) is

$$Q_a^{(t)}(\Sigma) = \sum_{i=0}^n -\frac{1}{2} \log(|\Sigma|) - \frac{1}{2} \sum_{j \in \mathcal{J}_i} \mathbb{E}_{\Sigma^{(t)}}[\mathbf{1}[M_i = j] | Z] W'_{ij} \Sigma^{-1} W_{ij}.$$

Working  $\mathbb{E}_{\Sigma^{(t)}}[\mathbf{1}[M_i = j] | Z] = \omega_{ij}$ , we see that  $Q_a^{(t)}$  is identical to  $Q^{(t)}$  given in (3.10), confirming that the “same”  $\Sigma$  parametrizes both the original data-generating process assumed in (3.1), and its degenerate approximation that we will use to make predictions (3.12). We may also think of maximizing  $Q$  as inferring motif instances given by the relation (3.13), *i.e.*, minimizing a distance metric.

The independent multivariate mixture distribution of  $\{Z_i\}$  considered here very easily provides  $k$ -step predictive distributions for  $k \leq p$ . If we have observed the process up to  $Y_n$  and wish to predict  $Y_{n+k}$ , this is equivalent to having observed  $Z$  up to  $Z_n$  and wishing to predict the last component of  $Z_{n+k}$ . Having observed  $Z_n$  completely, we have observed the first  $p - k + 1$  components of  $Z_{n+k}$ , and thus by the (misspecified) independence assumed for  $\{Z_i\}$ , the predictive distribution for  $Y_{n+k}$  depends only on these  $p - k + 1$  values. To write this, we denote  $\tilde{Z}_n^k$  as the first  $p - k + 1$  components of  $Z_{n+k}$  (or the last  $p - k + 1$  components of  $Z_n$ ); also let  $\tilde{W}_{nj}^k = \tilde{Z}_n^k - \tilde{Z}_j^k$  and partition  $\Sigma$  into  $\Sigma_{11}^k$  as the upper-left  $(p - k + 1) \times (p - k + 1)$  submatrix,  $\Sigma_{22}^k$  as the single bottom-right element (thus identical to  $\Sigma_{22}$ ), and  $\Sigma_{12}^k, \Sigma_{21}^k$  accordingly. Then we have

$$(3.14) \quad Y_{n+k} | Y_{(-m):n} \sim \sum_{j \in \mathcal{J}_{n+k}} \alpha_j^k N(\mu_j^k, \sigma_k^2),$$

where

- $\alpha_j^k = \mathbb{P}(M_{n+k} = j | \tilde{Z}_n^k) \propto \exp(-(\tilde{W}_{nj}^k)' [\Sigma_{11}^k]^{-1} \tilde{W}_{nj}^k / 2)$ .
- $\mu_j^k = Y_{n+k-j} + \Sigma_{21}^k [\Sigma_{11}^k]^{-1} \tilde{W}_{nj}^k$ .
- $\sigma_k^2 = \Sigma_{22}^k - \Sigma_{21}^k [\Sigma_{11}^k]^{-1} \Sigma_{12}^k$ .

In terms of motifs, these predictive distributions result from considering the most recent subseries of the data of length  $p - k + 1$  as a partially observed motif instance,  $Z_{n+k}$ , which includes the future observation we wish to predict,  $Y_{n+k}$ . Using the implied motif relation in (3.13), we infer both the motif for which  $Z_{n+k}$  is an instance, and derive predictive distributions using simple multivariate normal properties (3.14).

Of course, we use  $\hat{\Sigma}$ , the solution to (3.11), in place of  $\Sigma$  in the above expressions, acknowledging that the resulting predictive distributions fail to account for the uncertainty in our estimate of  $\Sigma$ .

**4. Evaluating out-of-sample prediction error with competing methods.** We compare out-of-sample prediction performance using the LMAR( $p, \Sigma$ ) model with two methods that are very straightforward to implement and compare favorably to alternative methods with regards to prediction accuracy (Sharp et al. [32], Krauss, Nill and Oelfke [18]).

1. *Feedforward neural networks.* Multilayer feedforward neural networks with at least one hidden layer have been used to forecast lung tumor motion by Murphy, Isaakson and Jalden [26] and Murphy and Dieterich [25], as well as in simultaneous comparisons of several methods [32, 18, 11]. We use  $p \times h \times 1$  neural networks, which predict  $Y_{n+k}$  as a function of  $Y_{(-m):n}$  as follows: let  $X_i = Y_{(i-p+1):i}$ . Then

$$(4.1) \quad \hat{Y}_{i+k} = \beta_0 + \beta' G(X_i),$$

where  $G(X_i) = (g(w_{01} + w'_1 X_i) \ g(w_{02} + w'_2 X_i) \ \dots \ g(w_{0h} + w'_h X_i))'$  with activation function  $g$ ; here we assume  $g(x) = 1/(1 + \exp(-x))$ . Hyperparameters  $p$  and  $h$  are set by the user (as is the form of the activation function). Unknown parameters  $\beta_0, \beta, w_{01}, \dots, w_{0h}, w_1, \dots, w_h$  are estimated by minimizing sum of squares using the R package **nnet** (Venables and Ripley [39]). Because the number of unknown parameters is large ( $w_1, \dots, w_h$  are  $p$ -vectors), to prevent overfitting, a regularization term is often used in the sum of squares minimization. Then, the model is fit by minimizing

$$(4.2) \quad C(Y, \theta) = \sum_{i=0}^{n-k} (\hat{Y}_{i+k} - Y_{i+k})^2 + \lambda \theta' \theta,$$

where  $\theta$  represents a vector of all unknown parameters stacked together, and  $\lambda$  is a penalty hyperparameter that is supplied by the user, with higher values providing more shrinkage.

2. *Ridge regression.* The second competing method considered is a linear predictor of the form

$$(4.3) \quad \hat{Y}_{i+k} = \beta_0 + \beta' X_i,$$

where  $\beta_0, \beta$  are found by minimizing

$$(4.4) \quad C(Y, \theta) = \sum_{i=0}^{n-k} (\hat{Y}_{i+k} - Y_{i+k})^2 + \lambda(\beta_0^2 + \beta' \beta).$$

Nearly all studies involving forecasting lung tumor motion consider predictors of this form, usually referred to as ridge regression. However, since ridge regression assumes  $\{Y_i\}$  to be independent (Hoerl and Kennard [14]), the model implied by (4.3)–(4.4) is better described as fitting an autoregressive model of order  $p + k - 1$  (the first  $k - 1$  coefficients being 0) using conditional least squares, with an  $L_2$  penalty on the vector of autoregressive coefficients (yet we shall refer to this prediction method as ridge regression).

Linear models lack many features that seem appropriate for this forecasting example, such as multimodal and/or heteroskedastic conditional distributions, yet still perform reasonably well and are commonly used as a baseline for comparing tumor prediction methods.

## 5. Lung tumor case study analysis.

5.1. *Data preprocessing.* Similar to Krauss, Nill and Oelfke [18], we use 80 seconds of data (2400 observations) from each time series, 40 seconds for model fitting, and 40 seconds for out-of-sample prediction given the model fit to the first 40 seconds of data. This necessitates removing time series for which we have fewer than  $2400 + k$  observations, where  $k$  is the forecast window. This eliminates 61 of the 171 time series in our data base, unfortunately including all time series from patients 1, 2, and 3. An additional 15 time series were eliminated because there were several gaps in the observation sequence. This leaves us with 95 total time series; patient 8 only has one time series, and patient 6 has the next fewest series with 9. Patient 11 has the most time series with 21.

Method	Hyperparameter	Description
LMAR	$p$	Motif length (3.13)
Neural Networks	$p$	Length of input vector $X_i$ (4.1)
	$h$	Number of neurons in hidden layer (4.1)
	$\lambda$	Shrinkage; L2 penalty (4.2)
Ridge Regression	$p$	Length of input vector $X_i$ (4.3)
	$\lambda$	Shrinkage; L2 penalty (4.4)

TABLE 2

List of global, patient-independent hyperparameters to be tuned for each prediction method

5.2. *Tuning hyperparameters.* Because of the need for real-time model fitting and prediction, all tuning and hyperparameters for the methods we consider must be specified prior to the administration of radiotherapy—before any data is observed. This suggests finding specifications for each model that perform reasonably well for all patients, though perhaps sub-optimally for each patient individually. Indeed, this is the approach usually taken in the literature [32, 18, 11]. Because patients are typically given several or many instances of radiotherapy during different sessions, there seems to be potential for more patient-specific tuning of hyperparameters, though this is left as a separate problem for now.

Table 2 lists the hyperparameters and/or tuning parameters for each of the prediction methods we consider. As described in section 5.1, since the first 40 seconds of each time series will not be used to evaluate out-of-sample prediction, we may use these subseries to find sensible, patient-independent values for all hyperparameters. Each 40 second subseries is further divided, where for a given set of hyperparameters each prediction method is fit to the first 30 seconds of data (900 observations), and then the remaining 10 seconds are used to generate out-of-sample predictions, for which we store the vector of errors.

Using a course grid search over the parameter space given in table 2, predictive error (both root mean squared error (RMSE), as well as median absolute error (MAE), which is more robust to heavy-tailed error distributions) is averaged across patients, allowing us to choose the best set of patient-independent hyperparameter values (Krauss, Nill and Oelfke [18]). Note that different hyperparameter values are chosen for different forecast windows.

5.3. *Computational considerations.* Ridge regression yields almost instantaneous estimates of parameters necessary for prediction ( $\beta$  in (4.3)),

since (4.4) can be minimized in closed form. Fitting neural networks (4.1), however, requires numerical optimization of (4.2). This was carried out using the `nnet` package in R, which implements the BFGS algorithm (Venables and Ripley [39]). Because (4.2) is not convex, we recommend several random starting points for initiating the optimization, insomuch as time allows; the dimension of the parameter space, as well as convergence criteria for the numerical optimization, are both extremely important considerations in addition to the length of the time series being fit. For example, on a Lenovo X220 laptop with an Intel Core i5-2520M 2.50 Ghz processor, a  $45 \times 6 \times 1$  neural network takes about 4 seconds to fit on 1200 observations when using `nnet`'s default convergence criteria, with 10 randomly initialized starting points.

The computation time in fitting the  $\text{LMAR}(p, \Sigma)$  depends critically on both the convergence criteria for the EM algorithm, as well as the initial value of  $\Sigma$  used. Typically, the likelihood (3.6) or log-likelihood is used; however, the EM updates given in (3.11) are only approximate, meaning the likelihood is not guaranteed to increase at every iteration. We found that using the approximate log-likelihood (3.9) to check convergence yielded convergence in the exact log-likelihood. This being the case, other metrics could possibly be used to check convergence that are quicker to calculate than (3.9), such as the Frobenius norm of differences in the updates of  $\hat{\Sigma}$ . To obtain good starting values, the algorithm can be run before having observed the entire training sequence, using a simple starting value of a diagonal matrix. Using a relative tolerance of 0.0001 for the approximate log-likelihood (a higher tolerance can surely be used), we were able to compute  $\hat{\Sigma}$  in no more than three seconds for each of the time series considered.

We used  $m = 400$ , though found essentially identical results for  $m = 200$  and  $m = 300$  (higher values of  $m$  favor faster, but less precise, estimation of  $\Sigma$ ).

**5.4. Results.** The measures of predictive performance we consider are RMSE, MAE, and several values of the empirical distribution function for absolute errors ( $\mathbb{P}(|\text{error}| < x)$ ). We report these quantities averaged over each of the 8 patients for which we consider predictions for a forecast window of 0.2s (6 observations) in table 3. The analogous results for a forecast window of 0.4s are in table 4, and those for a forecast window of 0.6s are in table 5.

We stress that RMSE may not be the most useful summary of predictive performance since the error distributions are heavy-tailed, and in the application of radiotherapy, we are more concerned with whether or not the

treatment beam was localized to the tumor than the squared distance of the treatment beam to the tumor<sup>2</sup>. For this reason, we feel the values of the distribution function for the error distribution of each method are the most useful comparison of the methods considered here. Ultimately, the dosimetric effects of these errors are of most interest, but their determination is complicated, and beyond the scope of this work.

Two further points of emphasis regarding the accuracy summaries are that while we eliminated time series with unevenly spaced observations from consideration, we still have quite a few time series with unusual motion in our data base. Without actually observing the patient, we are not sure whether observed deviations from normal breathing are caused by exogenous factors or are instances of relevant components of the data-generating process, such as coughs, yawns, deep breaths, etc. The other point is that there is a lot of disparity in the measures of predictive performance within the literature on this subject; in addition to working with different data sets, obtained from different equipments, some authors account for the between-patient variation in respiratory dynamics by scaling or normalizing all curves, or by comparing errors from a prediction method against errors from making no prediction and just using the lagged value of the series. When using evaluation procedures of Krauss, Nill and Oelfke [18] and Murphy and Dieterich [25], we are able to produce very similar results with ridge regression and linear models. However, the error summaries we present here, in comparison with the LMAR model, are not directly comparable to these results.

5.5. *Quantitative summaries.* Summarizing table 3, we see that the linear model (ridge regression) is actually sub-optimal in all accuracy measures for all patients, although for some patients (such as 6, 8, 9, 10) the performance is almost as good as neural networks (Krauss, Nill and Oelfke [18] observe this effect as well for some patients). LMAR seems to give the most accurate forecasts for patients 6, 7, 8, 9, 10, and 11; NNs perform the best for patient 4, and NNs and LMAR perform equally well for patient 5.

Table 4, for the results of the 0.4s forecast, tells a similar story, with ridge regression never outperforming both NNs and LMAR for any patient or error summary statistic, though comparable to NNs for patients 6, 8, 9, and 10. LMAR looks to be the most accurate for patients 6, 7, 9, 10, and 11, while neural networks do the best for patients 4, 5, and 8.

The results in table 5 (for the 0.6s forecast window) are once again similar. Ridge regression is never optimal for any patient or error summary statistic,

---

<sup>2</sup>However, the loss function implied in the model fitting and point prediction is squared error loss, which is the simplest for many computation reasons.

Patient	Method	RMSE	MAE	$\mathbb{P}(0.5)$	$\mathbb{P}(1.0)$	$\mathbb{P}(2.0)$	$\mathbb{P}(3.0)$	$\mathbb{P}(5.0)$
4	LMAR	0.52	0.24	0.77	0.93	0.99	1.00	1.00
	NNs	0.46	0.22	0.80	0.95	1.00	1.00	1.00
	Ridge	0.53	0.31	0.70	0.93	1.00	1.00	1.00
5	LMAR	0.56	0.25	0.74	0.92	0.99	1.00	1.00
	NNs	0.55	0.27	0.74	0.93	0.99	1.00	1.00
	Ridge	0.58	0.31	0.69	0.92	0.99	1.00	1.00
6	LMAR	0.77	0.40	0.59	0.85	0.98	1.00	1.00
	NNs	1.01	0.46	0.54	0.79	0.95	0.98	1.00
	Ridge	0.83	0.42	0.57	0.84	0.98	1.00	1.00
7	LMAR	0.40	0.15	0.89	0.96	1.00	1.00	1.00
	NNs	0.43	0.19	0.84	0.96	1.00	1.00	1.00
	Ridge	0.44	0.26	0.79	0.97	1.00	1.00	1.00
8	LMAR	1.27	0.62	0.43	0.69	0.91	0.97	0.99
	NNs	1.26	0.68	0.40	0.68	0.92	0.97	0.99
	Ridge	1.44	0.69	0.38	0.64	0.88	0.96	0.99
9	LMAR	0.58	0.22	0.79	0.92	0.99	1.00	1.00
	NNs	0.73	0.32	0.67	0.89	0.98	0.99	1.00
	Ridge	0.81	0.34	0.65	0.87	0.96	0.99	1.00
10	LMAR	0.88	0.36	0.63	0.85	0.97	0.99	1.00
	NNs	1.09	0.44	0.55	0.82	0.96	0.99	1.00
	Ridge	0.95	0.45	0.54	0.83	0.97	0.99	1.00
11	LMAR	1.13	0.44	0.54	0.77	0.92	0.97	1.00
	NNs	1.24	0.50	0.50	0.75	0.91	0.96	1.00
	Ridge	1.19	0.63	0.42	0.68	0.91	0.97	1.00

TABLE 3

*Summary of prediction errors for a forecast window of 0.2s ( $k = 6$  observations). RMSE is root mean squared error, MAE is median absolute error, and  $\mathbb{P}(x)$  is the proportion of absolute errors less than  $x$ .*

and the disparity is more evident in many of the patients than for shorter forecasting windows. LMAR does the best with this forecast window for patients 4, 6, 7, 10, and 11. Neural networks do the best with patient 8, and patients 5 and 9 have extremely similar prediction error summaries for both LMAR and NNs.

Another important consideration of predictive performance is the proportion of forecasted observations for which one prediction method achieves a lower error than the other two methods. In other words, this is the proportion of time each predicted time series is closest to the true time series. Table 6 gives these proportions for each patient/forecast window. We also provide the ratio of total absolute error to the minimum pointwise total ab-

Patient	Method	RMSE	MAE	$\mathbb{P}(0.5)$	$\mathbb{P}(1.0)$	$\mathbb{P}(2.0)$	$\mathbb{P}(3.0)$	$\mathbb{P}(5.0)$
4	LMAR	0.99	0.39	0.57	0.78	0.93	0.98	1.00
	NNs	0.90	0.39	0.59	0.80	0.95	0.99	1.00
	Ridge	1.08	0.62	0.41	0.70	0.93	0.98	1.00
5	LMAR	0.96	0.42	0.56	0.79	0.95	0.99	1.00
	NNs	0.89	0.40	0.58	0.81	0.96	0.99	1.00
	Ridge	1.01	0.56	0.46	0.73	0.94	0.99	1.00
6	LMAR	1.54	0.82	0.33	0.58	0.84	0.94	0.99
	NNs	1.74	0.93	0.29	0.53	0.79	0.91	0.99
	Ridge	1.59	0.88	0.30	0.55	0.83	0.94	0.99
7	LMAR	0.85	0.27	0.72	0.87	0.95	0.98	1.00
	NNs	0.88	0.36	0.62	0.82	0.95	0.99	1.00
	Ridge	1.00	0.59	0.44	0.73	0.94	0.99	1.00
8	LMAR	2.63	1.46	0.20	0.37	0.63	0.83	0.94
	NNs	2.71	1.27	0.22	0.42	0.66	0.80	0.93
	Ridge	2.86	1.54	0.19	0.35	0.59	0.75	0.93
9	LMAR	1.30	0.52	0.49	0.72	0.89	0.95	0.99
	NNs	1.69	0.64	0.41	0.67	0.86	0.93	0.97
	Ridge	1.68	0.73	0.37	0.63	0.85	0.93	0.98
10	LMAR	1.75	0.77	0.36	0.60	0.83	0.92	0.98
	NNs	2.18	0.93	0.31	0.53	0.78	0.90	0.97
	Ridge	1.86	0.94	0.28	0.53	0.81	0.92	0.98
11	LMAR	2.59	1.06	0.30	0.48	0.71	0.83	0.93
	NNs	2.95	1.19	0.25	0.44	0.67	0.79	0.92
	Ridge	2.69	1.51	0.19	0.36	0.61	0.77	0.93

TABLE 4

Summary of prediction errors for a forecast window of  $0.4s$  ( $k = 12$  observations). RMSE is root mean squared error, MAE is median absolute error, and  $\mathbb{P}(x)$  is the proportion of absolute errors less than  $x$ .

solute error among the three methods. Here again, we see LMAR performing very well for all forecast windows considered, particularly for patients 6, 7, 9, 10, and 11.

**5.6. Qualitative summaries.** When looking at the predicted time series for each method used, the general pattern we observe is that LMAR outperforms the other two methods when there are multiple different breath shapes present in the time series, such as was highlighted in figure 3. Figure 7 shows one (atypically dramatic) instance of such behavior. The top curve is the first 40 seconds of the time series, on which all prediction methods were trained. The next three curves give the predicted time series at a window



Patient	Method	RMSE	MAE	$\mathbb{P}(0.5)$	$\mathbb{P}(1.0)$	$\mathbb{P}(2.0)$	$\mathbb{P}(3.0)$	$\mathbb{P}(5.0)$
4	LMAR	1.17	0.43	0.54	0.73	0.91	0.97	1.00
	NNs	1.20	0.48	0.51	0.72	0.90	0.97	1.00
	Ridge	1.50	0.86	0.31	0.57	0.84	0.95	0.99
5	LMAR	1.16	0.52	0.49	0.71	0.92	0.97	1.00
	NNs	1.15	0.51	0.49	0.73	0.92	0.98	1.00
	Ridge	1.39	0.78	0.34	0.61	0.87	0.95	1.00
6	LMAR	2.00	1.06	0.26	0.48	0.75	0.88	0.97
	NNs	2.43	1.38	0.20	0.39	0.66	0.81	0.94
	Ridge	2.14	1.28	0.21	0.41	0.70	0.86	0.97
7	LMAR	1.23	0.42	0.56	0.77	0.90	0.95	0.99
	NNs	1.35	0.51	0.50	0.70	0.87	0.94	0.99
	Ridge	1.56	0.96	0.27	0.52	0.81	0.93	1.00
8	LMAR	3.57	2.01	0.15	0.28	0.50	0.67	0.88
	NNs	3.46	1.76	0.15	0.31	0.55	0.73	0.88
	Ridge	4.11	2.26	0.16	0.26	0.46	0.59	0.79
9	LMAR	2.05	0.92	0.31	0.53	0.78	0.88	0.96
	NNs	2.45	0.92	0.30	0.53	0.77	0.86	0.94
	Ridge	2.42	0.98	0.27	0.51	0.76	0.86	0.95
10	LMAR	2.56	1.19	0.25	0.44	0.69	0.82	0.94
	NNs	2.98	1.35	0.21	0.40	0.64	0.78	0.92
	Ridge	2.67	1.41	0.19	0.37	0.65	0.81	0.94
11	LMAR	3.70	1.50	0.26	0.40	0.57	0.69	0.86
	NNs	3.99	1.70	0.19	0.35	0.55	0.67	0.83
	Ridge	3.99	2.40	0.12	0.23	0.43	0.59	0.81

TABLE 5

Summary of prediction errors for a forecast window of 0.6s ( $k = 18$  observations). RMSE is root mean squared error, MAE is median absolute error, and  $P(x)$  is the proportion of absolute errors less than  $x$ .

of 0.4s for LMAR (red), NN (blue), and ridge regression (green). Since the prediction period starts with a very uncharacteristic series of breaths followed by pauses of varying lengths before the next inhale, both the period and shape of the time series are different during the beginning of the test sequence.

It is clear that the superior predictive performance for LMAR on this particular time series is due to the local self-similarity that's assumed in the model, as it's reasonable to assume every subseries of some fixed length (for a window of 0.4s, a value of  $p = 24$  was used for LMAR) is a motif instance. The other two methods suffer from the fact that in order to capture periodicity or self-similarity in the data, they need to consider larger values

Patient	Method	0.2s Forecast		0.4s Forecast		0.6s Forecast	
		%	Ratio	%	Ratio	%	Ratio
4	LMAR	0.35	1.93	<b>0.39</b>	1.81	<b>0.42</b>	<b>1.55</b>
	NNs	<b>0.39</b>	<b>1.71</b>	<b>0.39</b>	<b>1.67</b>	0.36	1.61
	Ridge	0.26	2.16	0.22	2.22	0.22	2.26
5	LMAR	<b>0.37</b>	<b>1.92</b>	0.36	1.91	<b>0.37</b>	1.74
	NNs	0.33	<b>1.92</b>	<b>0.37</b>	<b>1.78</b>	0.36	<b>1.71</b>
	Ridge	0.29	2.13	0.27	2.19	0.27	2.25
6	LMAR	<b>0.37</b>	<b>1.74</b>	<b>0.38</b>	<b>1.70</b>	<b>0.41</b>	<b>1.54</b>
	NNs	0.30	2.15	0.29	1.94	0.27	1.92
	Ridge	0.34	1.81	0.33	1.77	0.33	1.71
7	LMAR	<b>0.43</b>	<b>1.79</b>	<b>0.47</b>	<b>1.67</b>	<b>0.46</b>	<b>1.50</b>
	NNs	0.32	2.09	0.33	1.94	0.34	1.74
	Ridge	0.24	2.37	0.20	2.50	0.20	2.37
8	LMAR	<b>0.38</b>	<b>1.68</b>	<b>0.37</b>	1.88	0.36	1.68
	NNs	0.35	1.70	0.36	<b>1.87</b>	<b>0.37</b>	<b>1.58</b>
	Ridge	0.27	1.91	0.27	2.08	0.26	1.96
9	LMAR	<b>0.45</b>	<b>1.80</b>	<b>0.42</b>	<b>1.80</b>	<b>0.38</b>	<b>1.79</b>
	NNs	0.29	2.37	0.31	2.26	0.32	1.99
	Ridge	0.26	2.61	0.27	2.36	0.31	2.01
10	LMAR	<b>0.41</b>	<b>1.91</b>	<b>0.40</b>	<b>1.85</b>	<b>0.38</b>	<b>1.78</b>
	NNs	0.30	2.24	0.30	2.24	0.31	2.07
	Ridge	0.29	2.13	0.30	2.03	0.31	1.93
11	LMAR	<b>0.40</b>	<b>1.87</b>	<b>0.41</b>	<b>1.84</b>	<b>0.43</b>	<b>1.69</b>
	NNs	0.33	2.05	0.32	2.09	0.32	1.88
	Ridge	0.27	2.22	0.27	2.16	0.25	2.09

TABLE 6

Summary of predictive performance of all three methods at all three forecast windows. % refers to the proportion of predictions for each patient for which the corresponding method had the lowest absolute error. Ratio represents the sum of total errors for a particular method divided by the minimum prediction error for each point across all three methods. A value of 1.0 means that one particular method achieved uniformly lower predictive error than the other methods.

of  $p$  (for this forecast window,  $p = 45$  was used for the neural networks and  $p = 85$  for ridge regression), which will inflate prediction error when the data undergo structural shifts such as a change or weakening in periodicity.

When the time series are more well-behaved, all three methods perform quite well; in fact, neural networks tend to have the lowest errors when all three curves are accurate. Figure 8 shows the training and prediction test series for a stable, though unusual looking respiratory trace. We should ex-

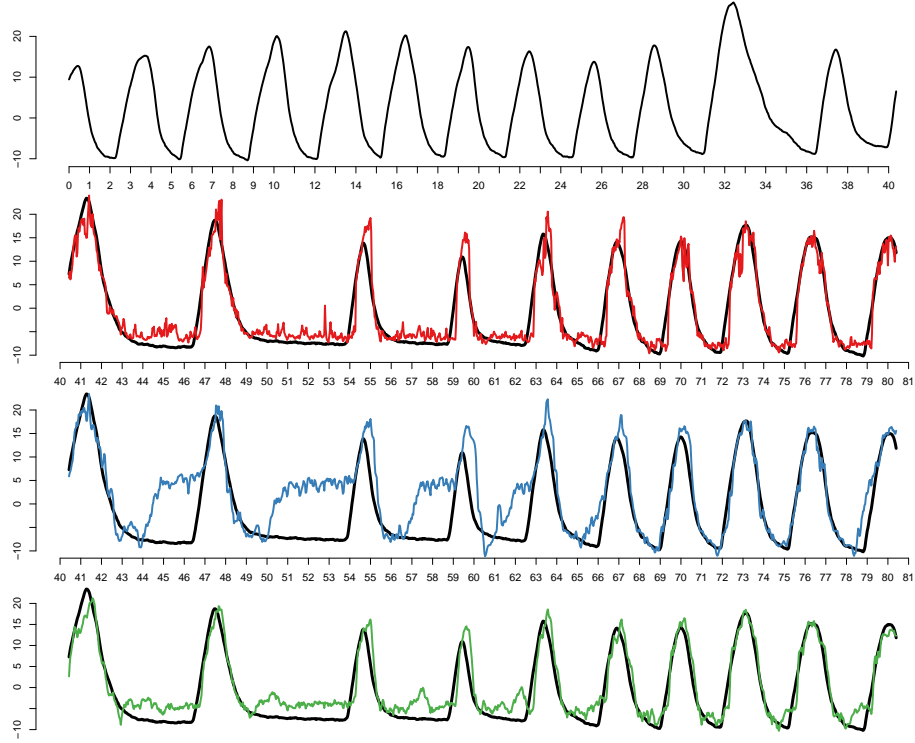


FIG 7. Predictions for patient 11, day 7 beam 2 using a forecast window of  $0.4s$  (12 observations). The  $40s$  training sequence is at top, with LMAR predictions in red, NN predictions in blue, and ridge regression predictions in green.

pect the performance of neural networks to be superior when the dynamics of the tumor motion are stable, as the parameter space for neural networks is far larger; in theory, feedforward neural networks with at least one hidden layer can approximate any continuous function arbitrarily well (Hornik, Stinchcombe and White [15]), including time series prediction. Yet, when they are not stable, neural networks are limited compared with LMAR in that the form of the dependence on the most recent  $p$  observations cannot evolve.

The neural network forecasting method of Murphy and Dieterich [25] continuously retrain the neural network using the updated history of the time series. While they do not compare this to the alternative of not actively updating the model, Krauss, Nill and Oelfke [18] do so and find a small improvement in RMSE of about 1–3%.

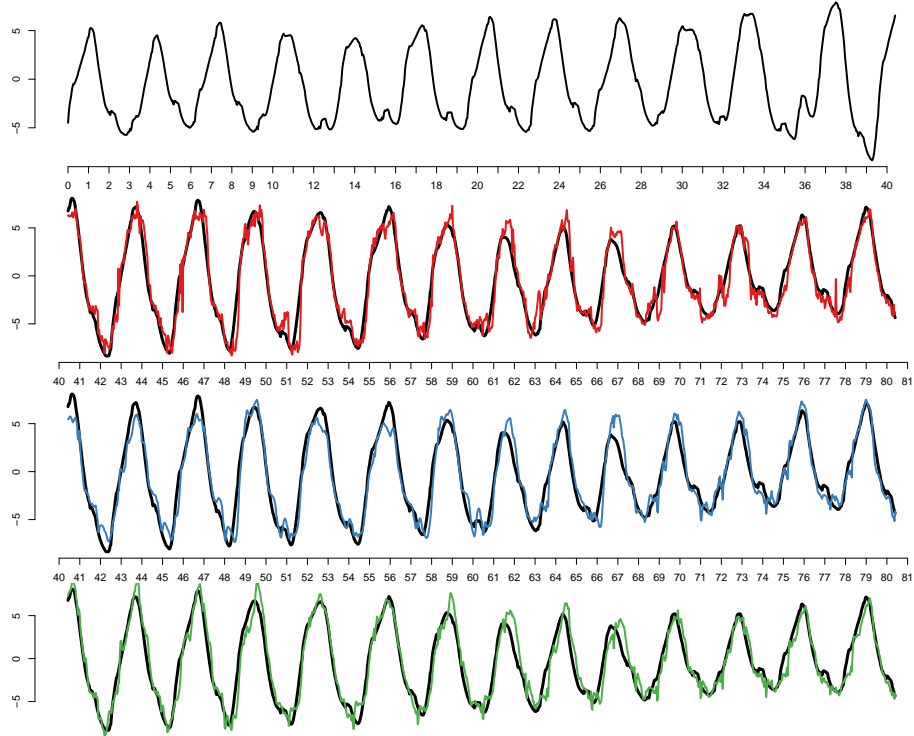


FIG 8. Predictions for patient 9, day 2 beam 2 using a forecast window of 0.4s (12 observations). The 40s training sequence is at top, with LMAR predictions in red, NN predictions in blue, and ridge regression predictions in green.

**6. Discussion.** The location-mixture autoregressive (LMAR) model introduced in this paper provides accurate, real-time forecasts of lung tumor motion. Our method achieves better performance on out-of-sample prediction for forecasts windows of 0.2s, 0.4s, and 0.6s for the majority of the patients considered than existing methods such as neural networks (which performed best in a prediction comparison study of Krauss, Nill and Oelfke [18]) and penalized linear models (a common baseline for judging predictive performance). We also note that uncertainty quantification is quite straightforward using our model, where as it is hard to do using neural networks.

The LMAR model is similar to other autoregressive models that yield multimodal conditional distributions, such as the class of threshold autoregressive models [34], yet the parameter space consists of just a single, low-dimensional covariance matrix, and the model admits accurate closed-form approximations of multiple-step ahead predictive distributions. The LMAR

model also has a useful interpretation in the context of time series motifs, which can describe the data-generating process and the form of forecasts.

While the predictive performance of our method on this data set is very encouraging, the parameter inference for the LMAR model presented here is approximate, and the assumptions of both the model and its inference may not be appropriate for some other non-linear time series. Formalizing and generalizing the LMAR model is thus a fruitful area for future work.

Real-time prediction of lung tumor motion presents additional challenges to those presented in this work. It is preferable to have as short a training window as possible, since during this time the patient may be irradiated without actually receiving the benefit of tumor tracking. While some training is actually necessary to estimate the system latency in some cases (we have treated it as fixed throughout this work), the 40 seconds used for training in this paper (while typical in the literature on the subject) could ideally be reduced.

Also, one can consider patient-specific hyperparameter values and/or tuning parameters or modify the model to borrow information across the patients. Because of the need for real-time model fitting before we can forecast, it is most likely infeasible to apply any model selection criteria (either within-model, such as for hyperparameters, or between-model) after having begun to observe data. More study of between-patient and within-patient variability in model fits could help researchers use more patient-optimal prediction methods (as well as begin prediction after a shorter training sequence, as they wouldn't need to rely solely on the observed data for parameter estimation).

The parametric simplicity of the LMAR model, as well as its formalization as a statistical model as opposed to a prediction algorithm, enable generalizations of our procedure to include hierarchical models and other statistical structures that address the challenges of delivering accurate external beam radiotherapy. Combined with its excellent predictive performance on real data, the LMAR model represents a promising new contribution to this area of research.

**Acknowledgements.** The authors would like to thank Dr. Seiko Nishioka of the Department of Radiology, NTT Hospital, Sapporo, Japan and Dr. Hiroki Shirato of the Department of Radiation Medicine, Hokkaido University School of Medicine, Sapporo, Japan for sharing the patient tumor motion dataset with us. The project described was supported by Award Numbers RSCH1206 (JHL) from the Radiological Society of North America and R21CA156068 (RIB) from the National Cancer Institute. NSP is par-

tially supported by the NSF grant DMS 1107070. The content is solely the responsibility of the authors and does not necessarily represent the official views of the National Cancer Institute, National Science Foundation or the National Institutes of Health.

## References.

- [1] BERBECO, R. I., NISHIOKA, S., SHIRATO, H., CHEN, G. T. and JIANG, S. B. (2005). Residual motion of lung tumours in gated radiotherapy with external respiratory surrogates. *Physics in medicine and biology* **50** 3655.
- [2] BOSHNAKOV, G. N. (2009). Analytic expressions for predictive distributions in mixture autoregressive models. *Statistics & Probability Letters* **79** 1704–1709.
- [3] CARVALHO, A. X. and TANNER, M. A. (2005). Mixtures-of-experts of autoregressive time series: asymptotic normality and model specification. *Neural Networks, IEEE Transactions on* **16** 3956.
- [4] CHIU, B., KEOGH, E. and LONARDI, S. (2003). Probabilistic discovery of time series motifs. In *Proceedings of the ninth ACM SIGKDD international conference on Knowledge discovery and data mining* 493498.
- [5] D D’SOUZA, W., NAQVI, S. A. and CEDRIC, X. Y. (2005). Real-time intra-fraction-motion tracking using the treatment couch: a feasibility study. *Physics in medicine and biology* **50** 4021.
- [6] DAS, G., LIN, K.-I., MANNILA, H., RENGANATHAN, G. and SMYTH, P. (1998). Rule Discovery from Time Series. In *KDD* **98** 16–22.
- [7] DE GOOIJER, J. G. and KUMAR, K. (1992). Some recent developments in non-linear time series modelling, testing, and forecasting. *International Journal of Forecasting* **8** 135156.
- [8] DEMPSTER, A. P., LAIRD, N. M. and RUBIN, D. B. (1977). Maximum likelihood from incomplete data via the EM algorithm. *Journal of the Royal Statistical Society. Series B (Methodological)* 138.
- [9] ERNST, F., SCHLAEFER, A. and SCHWEIKARD, A. (2007). Prediction of respiratory motion with wavelet-based multiscale autoregression. In *Medical Image Computing and Computer-Assisted Intervention–MICCAI 2007* 668–675. Springer.
- [10] ERNST, F. and SCHWEIKARD, A. (2009). Forecasting respiratory motion with accurate online support vector regression (SVRpred). *International Journal of Computer Assisted Radiology and Surgery* **4** 439–447.
- [11] ERNST, F., DÜRICHEN, R., SCHLAEFER, A. and SCHWEIKARD, A. (2013). Evaluating and comparing algorithms for respiratory motion prediction. *Physics in medicine and biology* **58** 3911.
- [12] FU, T.-C. (2011). A review on time series data mining. *Engineering Applications of Artificial Intelligence* **24** 164–181.
- [13] HAMILTON, J. D. (1989). A new approach to the economic analysis of nonstationary time series and the business cycle. *Econometrica: Journal of the Econometric Society* 357384.
- [14] HOERL, A. E. and KENNARD, R. W. (1970). Ridge regression: Biased estimation for nonorthogonal problems. *Technometrics* **12** 55–67.
- [15] HORNIK, K., STINCHCOMBE, M. and WHITE, H. (1989). Multilayer feedforward networks are universal approximators. *Neural networks* **2** 359–366.
- [16] KALBFLEISCH, J. D. and SPROTT, D. A. (1970). Application of likelihood methods to models involving large numbers of parameters. *Journal of the Royal Statistical Society. Series B (Methodological)* 175–208.

- [17] KALET, A., SANDISON, G., WU, H. and SCHMITZ, R. (2010). A state-based probabilistic model for tumor respiratory motion prediction. *Physics in Medicine and Biology* **55** 7615.
- [18] KRAUSS, A., NILL, S. and OELFKE, U. (2011). The comparative performance of four respiratory motion predictors for real-time tumour tracking. *Physics in medicine and biology* **56** 5303.
- [19] KROLZIG, H.-M. (2000). Predicting Markov-Switching Vector Autoregressive Processes Technical Report, University of Oxford, Department of Economics.
- [20] LAU, J. W. and SO, M. K. (2008). Bayesian mixture of autoregressive models. *Computational Statistics & Data Analysis* **53** 3860.
- [21] LE, N. D., MARTIN, R. D. and RAFTERY, A. E. (1996). Modeling Flat Stretches, Bursts Outliers in Time Series Using Mixture Transition Distribution Models. *Journal of the American Statistical Association* **91** 15041515.
- [22] LIN, J., LONARDI, S., KEOGH, E. and PATEL, P. (2002). Finding motifs in time series. In *Proc. of the 2nd Workshop on Temporal Data Mining* 5368.
- [23] MCCULLOCH, R. E. and TSAY, R. S. (1994). Statistical analysis of economic time series via Markov switching models. *Journal of time series analysis* **15** 523–539.
- [24] MUEEN, A., KEOGH, E. J., ZHU, Q., CASH, S. and WESTOVER, M. B. (2009). Exact Discovery of Time Series Motifs. In *SDM* 473484.
- [25] MURPHY, M. J. and DIETERICH, S. (2006). Comparative performance of linear and nonlinear neural networks to predict irregular breathing. *Physics in Medicine and Biology* **51** 5903.
- [26] MURPHY, M. J., ISAAKSON, M. and JALDEN, J. (2002). Adaptive filtering to predict lung tumor motion during free breathing. In *CARS 2002 Computer Assisted Radiology and Surgery* 539–544. Springer.
- [27] RIAZ, N., SHANKER, P., WIERSMA, R., GUDMUNDSSON, O., MAO, W., WIDROW, B. and XING, L. (2009). Predicting respiratory tumor motion with multi-dimensional adaptive filters and support vector regression. *Physics in Medicine and Biology* **54** 5735.
- [28] ROTTMANN, J., KEALL, P. and BERBECO, R. (2013). Markerless EPID image guided dynamic multi-leaf collimator tracking for lung tumors. *Physics in medicine and biology* **58** 4195.
- [29] RUAN, D. and KEALL, P. (2010). Online prediction of respiratory motion: multidimensional processing with low-dimensional feature learning. *Physics in Medicine and Biology* **55** 3011.
- [30] SCHLÜTER, T. and CONRAD, S. (2012). Hidden markov model-based time series prediction using motifs for detecting inter-time-serial correlations. In *Proceedings of the 27th Annual ACM Symposium on Applied Computing. SAC '12* 158164. ACM, New York, NY, USA.
- [31] SCHWEIKARD, A., GLOSSER, G., BODDULURI, M., MURPHY, M. J. and ADLER, J. R. (2000). Robotic motion compensation for respiratory movement during radiosurgery. *Computer Aided Surgery* **5** 263–277.
- [32] SHARP, G. C., JIANG, S. B., SHIMIZU, S. and SHIRATO, H. (2004). Prediction of respiratory tumour motion for real-time image-guided radiotherapy. *Physics in medicine and biology* **49** 425.
- [33] TANAKA, Y., IWAMOTO, K. and UEHARA, K. (2005). Discovery of time-series motif from multi-dimensional data based on MDL principle. *Machine Learning* **58** 269–300.
- [34] TONG, H. (1978). *On a threshold model* **29**. Sijthoff & Noordhoff.
- [35] TONG, H. (1990). *Non-linear time series: a dynamical system approach*. Oxford University Press.

- [36] TONG, H. and LIM, K. S. (1980). Threshold autoregression, limit cycles and cyclical data. *Journal of the Royal Statistical Society. Series B (Methodological)* 245292.
- [37] TONG, H. and MOEANADDIN, R. (1988). On Multi-Step Non-Linear Least Squares Prediction. *Journal of the Royal Statistical Society. Series D (The Statistician)* **37** 101–110. ArticleType: research-article / Issue Title: Special Issue: Statistical Forecasting and Decision-Making / Full publication date: 1988 / Copyright 1988 Royal Statistical Society.
- [38] TRUONG, C. D. and ANH, D. T. (2012). Time Series Prediction Using Motif Information. In *Multi-disciplinary Trends in Artificial Intelligence* 110121. Springer.
- [39] VENABLES, W. N. and RIPLEY, B. D. (2002). *Modern Applied Statistics with S*, Fourth ed. Springer, New York. ISBN 0-387-95457-0.
- [40] WONG, C. S. and LI, W. K. (2000). On a mixture autoregressive model. *Journal of the Royal Statistical Society: Series B (Statistical Methodology)* **62** 95115.
- [41] YE, L. and KEOGH, E. (2009). Time series shapelets: a new primitive for data mining. In *Proceedings of the 15th ACM SIGKDD international conference on Knowledge discovery and data mining* 947–956. ACM.